Femtosecond resolution of ligand-heme interactions in the high-affinity quinol oxidase *bd*: A di-heme active site?

Marten H. Vos[†‡], Vitaliy B. Borisov[§], Ursula Liebl[†], Jean-Louis Martin[†], and Alexander A. Konstantinov[§]

[†]Institut National de la Santé et de la Recherche Médicale U451, Laboratoire d'Optique Appliquée, Ecole Polytechnique-École Nationale Supérieure des Techniques Avancées, 91761 Palaiseau Cedex, France; and [§]A. N. Belozersky Institute of Physico-Chemical Biology, Moscow State University, Moscow 119899, Russia

Communicated by Hans Frauenfelder, Los Alamos National Laboratory, Los Alamos, NM, December 6, 1999 (received for review October 25, 1999)

Interaction of the two high-spin hemes in the oxygen reduction site of the *bd*-type quinol oxidase from *Escherichia coli* has been studied by femtosecond multicolor transient absorption spectroscopy. The previously unidentified Soret band of ferrous heme b_{595} was determined to be centered around 440 nm by selective excitation of the fully reduced unliganded or CO-bound cytochrome *bd* in the α-band of heme b_{595}. The redox state of the *b*-type hemes strongly affects both the line shape and the kinetics of the absorption changes induced by photodissociation of CO from heme *d*. In the reduced enzyme, CO photodissociation from heme *d* perturbs the spectrum of ferrous cytochrome b_{595} within a few ps, pointing to a direct interaction between hemes b_{595} and *d*. Whereas in the reduced enzyme no heme *d*-CO geminate recombination is observed, in the mixed-valence CO-liganded complex with heme b_{595} initially oxidized, a significant part of photodissociated CO does not leave the protein and recombines with heme *d* within a few hundred ps. This caging effect may indicate that ferrous heme b_{595} provides a transient binding site for carbon monoxide within one of the routes by which the dissociated ligand leaves the protein. Taken together, the data indicate physical proximity of the hemes *d* and b_{595} and corroborate the possibility of a functional cooperation between the two hemes in the dioxygen-reducing center of cytochrome *bd*.

Reduction of molecular oxygen to water is a key step in aerobic energy production in living organisms, catalyzed by terminal oxidases. Although the mitochondrial respiratory chain ends invariably with an aa_3-type cytochrome *c* oxidase, a plethora of terminal oxidases is found within the bacterial kingdom. Most of these different enzymes display a large degree of sequence homology and belong to a superfamily of heme/copper oxidases (1), where a copper ion (Cu_B) is believed to cooperate with a high-spin heme in the reduction of dioxygen to water and may be directly involved in the redox-linked transmembrane proton pumping by the enzyme (2–8).

A very different class of oxygen-reactive respiratory enzymes is constituted by the *bd*-type quinol oxidases, which do not display homology to heme/copper oxidases or to any other protein (9, 10). The *bd*-type oxidases are found in a wide variety of bacteria and are of great physiological significance for survival under low oxygen ("microaerobic") conditions. The enzyme carries out the same chemical reaction as the heme-copper quinol oxidases, and at least some of the oxygen intermediates formed are analogous to those produced in the catalytic cycle of the heme-copper oxidases (11, 12). However, this process is not coupled to proton pumping (13), and the structure and composition of *bd*-type oxidases are quite different from those of heme/copper oxidases (reviewed in refs. 10 and 14).

Cytochrome *bd*, as purified from *Escherichia coli* or *Azotobacter vinelandii*, consists of two different subunits, both of which are integral membrane proteins. The three heme groups in the protein complex are located close to the outer surface of the bacterial membrane (9), and no other metals have been found so far. A low-spin heme *b* (b_{558}) is probably the electron entry site close to the quinol-binding domain (9, 15). High-spin heme *d* serves as an oxygen anchor and is assumed to be the site where O_2 is reduced to water. The functional role of the second high-spin heme, heme b_{595}, has not been well defined. It may act as electron carrier between heme b_{558} and heme *d* (16, 17), or it may be a functional analog of Cu_B in the heme-copper oxidases (18, 19). Arguments in favor of heme *d*–heme b_{595} proximity come from experiments demonstrating, at cryogenic temperatures, CO transfer to heme b_{595} on a time scale of hours after photodissociation from heme *d* in the membrane-bound cytochrome *bd* (19).

Ultrafast spectroscopy in the femtosecond regime offers a unique possibility to monitor in real time both structural and electronic dynamics associated with the initially localized perturbation (20), here caused by photodissociation of a ligand. We have undertaken a systematic femtosecond/picosecond study of the *bd*-type quinol oxidase from *E. coli* by varying the redox and ligation conditions. The measurements were performed both in the α-band, where the heme absorptions are well separated but weak for heme b_{595}, and in the strong Soret band, where the individual bands of the three hemes have not been resolved so far (14) and the interpretation of absorption changes is controversial. Here we focus on the results relevant to heme b_{595} (a detailed account of the entire study will be given elsewhere). We have identified the absorption band of this redox center in the Soret and, by monitoring ultrafast absorption changes in this region, have been able to show that heme b_{595} interacts with heme *d* and possibly can act as a transient binding site for CO after photodissociation of the ligand from heme *d*. The data favor proximity of the two hemes and hence their potential cooperation in oxygen reduction.

Materials and Methods

Materials. *N*-lauroylsarcosinate was from Fluka; sodium dithionite was from Merck; and *N*-dodecyl-*N*,*N*-dimethylammonio-3-propane-sulfonate (SB-12) was from Sigma. Other basic chemicals and biochemicals were commercial products of high purity from Sigma, Serva, Fluka, Merck, and Air Liquide (Grigny, France).

E. coli cells (strain GO 105/pTK1; ref. 21) overproducing cytochrome *bd* and deleted in cytochrome bo_3, kindly provided by R. Gennis (University of Illinois, Urbana-Champaign) were grown in 10-liter flasks at 37°C in a medium containing 80 mM potassium phosphate, 2.5 mM sodium citrate, 19 mM ammo-

Abbreviations: R, fully reduced; MV, mixed valence.

[‡]To whom reprint requests should be addressed. E-mail: vos@enstay.ensta.fr.

The publication costs of this article were defrayed in part by page charge payment. This article must therefore be hereby marked "*advertisement*" in accordance with 18 U.S.C. §1734 solely to indicate this fact.

Article published online before print: *Proc. Natl. Acad. Sci. USA*, 10.1073/pnas.030528197. Article and publication date are at www.pnas.org/cgi/doi/10.1073/pnas.030528197

nium sulfate, 1% tryptone, 0.5% yeast extract, 0.5% casamino acids, 0.01% L-tryptophan, 2% glycerol (vol/vol), 0.8 mM $MgSO_4$, 0.18 mM $FeSO_4 \cdot 7\,H_2O$, 0.1 mM $CuSO_4 \cdot 5\,H_2O$, 0.005% kanamycin, and 0.01% ampicillin, pH 7.2. Cytochrome *bd* was isolated from cell membranes as described (22) but the final hydroxylapatite chromatography step was omitted. Its concentration was determined from the dithionite-reduced minus air-oxidized difference absorption spectra by using a value of $\Delta\varepsilon_{628-607}$ of 10.8 $mM^{-1} \cdot cm^{-1}$ (23).

Sample Preparation. All measurements were made at room temperature in a buffer containing 50 mM *N*-(2-hydroxyethyl)piperazine-*N*′-(2-ethanesulfonate)/50 mM 2-(*N*-cyclohexylamino)-ethanesulfonate (pH 8), 0.5 mM EDTA, and 0.025% sodium *N*-lauroylsarcosinate in a 1-mm optical pathway cell at 21 μM of cytochrome *bd*. Experiments have been carried out with four basic stable states: (*a*) the "as isolated" form, which is mainly an oxycomplex (Oxy, $b_{558}{}^{3+}b_{595}{}^{3+}d^{2+}$-$O_2$); (*b*) the fully reduced (50 mM dithionite) unliganded state (R, $b_{558}{}^{2+}b_{595}{}^{2+}d^{2+}$); (*c*) the carbon monoxide complex of the fully reduced state (R-CO, $b_{558}{}^{2+}b_{595}{}^{2+}d^{2+}$-CO, obtained by bubbling with 1 mM CO) and (*d*) the carbon monoxide complex of the so-called "mixed valence" state (MV-CO, $b_{558}{}^{3+}b_{595}{}^{3+}d^{2+}$-CO, obtained by oxidation of the enzyme in the R-CO state with small quantities of air.

Spectroscopy. Absolute absorption spectra of the samples were recorded before and after the measurements in a Shimadzu UV-Vis 1601 spectrophotometer. Multicolor femtosecond absorption spectroscopy (24) was performed at a repetition rate of 30 Hz with compressed white light continuum probe pulses, and pump pulses centered at 590 nm [55 fs full width half maximum (fwhm)], 620 nm (70 fs fwhm), or 653 nm (70 fs fwhm). The sample was continuously moved perpendicular to the beams. Global exponential fitting of the data in terms of decay-associated spectra was performed with a procedure described previously (25) involving singular value decomposition and deconvolution with the instrument response function.

Results

The ground state optical absorption spectra of cytochrome *bd* in different states studied in this work were in general agreement with those published in the literature and did not change significantly during the measurements. The respective Soret regions are represented in Fig. 1*A*.

Resolution of Ferrous Heme b_{595} Soret Band. Fig. 1*B* shows the spectral evolution of the Soret band of fully reduced unliganded cytochrome *bd* (five representative spectra are shown), induced by excitation at 590 nm, close to the α-absorption maximum of ferrous heme b_{595}. During the first $\approx$0.5 ps, the difference spectra are dominated by a loss of absorbance at 438 nm. This bleaching then partly recovers, and the absorption changes transform to derivative-shaped spectra on the ps time scale, indicating a red-shift of a band centered around 440 nm. Global analysis of the entire spectra set assuming exponential decays resolves two major phases with time constants of 460 fs and 4 ps. Decay components with similar time constants were observed in experiments with other hemeproteins (24). The spectra associated with the major sub-ps decay phase observed in experiments at different redox and ligation states of cytochrome *bd* are shown in Fig. 1*C*.

In principle, the decay-associated spectra must include a contribution of excited-state absorption. However, for the fast-decaying excited state (e.g., the 460-fs component in the fully reduced cytochrome *bd*), presumably analogous to the Hb_I* state in hemoglobin (26), this absorption is weak and shifted rather far to the red (not shown, cf. ref. 26); therefore its contribution does not significantly distort the line shape of the band associated with bleaching of the ground state. This is not the case for the slower decaying excited state, which clearly has a bandshift-type spectrum (e.g., Fig. 1*B*, spectra at 1.4 and 2 ps; cf. ref. 26).

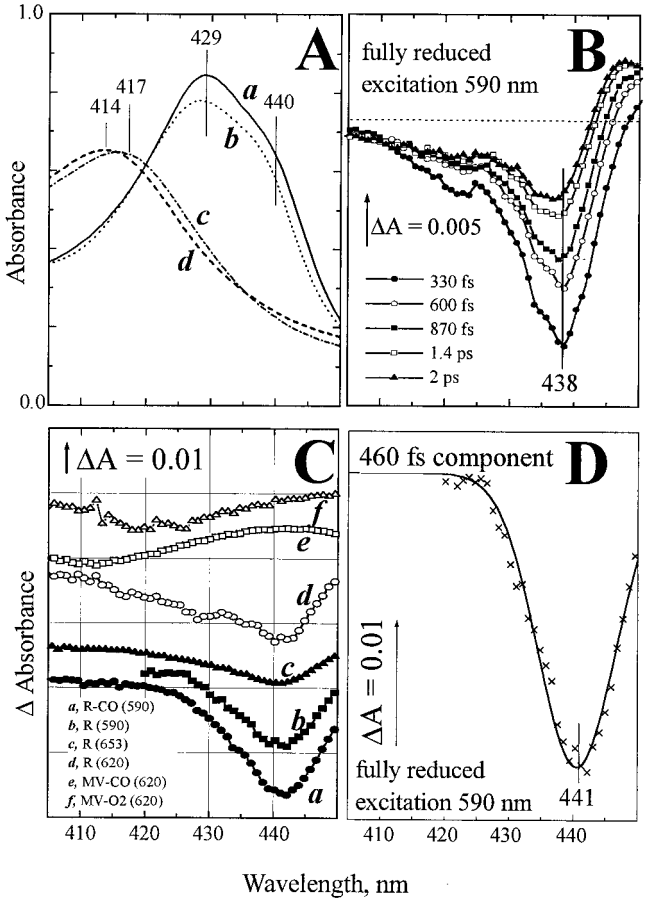

Fig. 1. Absorption characteristics of cytochrome *bd* in the Soret band. (*A*) Static absorption spectra of cytochrome *bd*: (*a*) fully reduced; (*b*) CO complex of the fully reduced state; (*c*) as-prepared oxygenated state; (*d*) CO complex of the MV state. (*B*) Evolution of spectral changes induced by femtosecond excitation of the fully reduced cytochrome *bd* at 590 nm. The difference spectra have been recorded versus the static R state at the indicated time intervals after the photoexcitation. (*C*) Spectra of the subpicosecond component (0.45–0.9 ps for different states) of the photobleaching induced in various states of cytochrome *bd*. Experiments have been carried out in the indicated redox and ligand binding states at λ_{exc} indicated in brackets. Solid line overlaying spectrum *b*: approximation with a single Gaussian. (*D*) γ-Absorption band of ferrous heme b_{595} resolved by photobleaching of the R state with 590-nm excitation (crosses, redrawn from *C*, curve *b*) has been approximated by a single Gaussian (solid line *a*).

The spectrum associated with the 460-fs decay component of photobleaching in the fully reduced enzyme excited at 590 nm is shown separately (Fig. 1*D*) and represents essentially bleaching of a band centered at $\approx$441 nm that can be described reasonably well by a Gaussian (solid line). We assign this spectrum to bleaching of the Soret band of ferrous heme b_{595}. First, with excitation of the fully reduced cytochrome *bd* at 653 nm, far from the α-maximum of ferrous b_{595}, the photobleaching at 441 nm strongly attenuates (compare spectra *b* and *c* in Fig. 1*C*). With excitation at 620 nm (Fig. 1*C* spectrum *d*), the bleaching of the 441-nm band was intermediate between excitation at 590 nm and 653 nm, and significant broadening on the blue side was observed, probably associated with a contribution of heme *d*.

Second, virtually the same photobleaching of the 441 band is observed for a CO complex of the fully reduced cytochrome *bd* (Fig. 1*C*, spectrum *a*), indicating that changes in the absorption characteristics of ferrous heme *d* induced by CO binding do not affect photobleaching of the 441-nm band. Third, this band is missing in the MV-CO and Oxy complexes of the enzyme where heme b_{595} is oxidized (Fig. 1*C*, spectra *e* and *f*). The Soret band of heme b_{595} as resolved in this work is centered at about the same wavelength as that of ferrous cytochrome *c* peroxidase [a high-spin heme *b*-containing enzyme (27) used earlier as a model for the absorption characteristics of heme b_{595} in the α,β-region (28)]; however, the peroxidase spectrum is much broader.

Photodissociation of Carbon Monoxide in the R and MV States. Figs. 2 and 3 compare photodissociation spectra of the CO complexes of the R-CO and MV-CO states. Both the line shape and the dynamics of the spectral changes are strikingly different in the two complexes.

The difference spectra of CO photodissociation observed in the Soret for the R-CO state of cytochrome *bd* after completion of the electronic relaxations are shown in Fig. 2*A*. The line shape of the absorption changes with the two extrema at 425 nm and 442 nm resembles the (mirrored) static difference spectrum induced by CO binding to reduced cytochrome *bd* with its characteristic (but poorly understood) W-form (e.g., refs. 23 and 29), as well as the difference spectrum of the rapid (microsecond) phase of CO recombination with the fully reduced cytochrome *bd* from *A. vinelandii* (30).

In contrast, the response of the MV-CO complex is characterized by a less complex difference spectrum, corresponding to an increased broad absorption band with a maximum in the range of 431 to 434 nm (Figs. 2*B* and 3*A*). We attribute this band to transiently generated ligand-free ferrous heme *d*. This report shows the absorption changes induced by CO in the Soret band of MV cytochrome *bd*. Transient spectra in the 550- to 660-nm range have been reported on the microsecond/millisecond time scale (15) but did not reveal any difference with respect to the R-CO state (in agreement with our ultrafast measurements in the α-band, data not shown), presumably because of the weak or broad contribution of heme b_{595} in this region. It must be emphasized that photodissociation of the MV-CO complex is followed by partial dislocation ("backflow") of electrons from ferrous heme *d* to ferric hemes *b* at a rate of 3,000 s^{-1} (15), which complicates resolution of the genuine photodissociation-linked spectral changes in experiments on a millisecond or microsecond time scale. These secondary changes can be neglected on the picosecond time scale.

A second striking difference between the R-CO and MV-CO states concerns the dynamics of the absorption changes induced by CO photodissociation. In the R-CO complex, the changes attain a stable level after relaxation of the electronic excited states in ≈20 ps so that the difference spectra recorded at 20 and 250 ps after the flash do not differ significantly (Fig. 2*A*). In contrast, the photoinduced changes observed in the MV-CO complex decrease by about one-half in this time range (Fig. 2 *B* and *C*). The line shape of the decay phase (spectrum *c* in Fig. 2*B*) is similar to that of the initial photoinduced spectral changes. Within a maximal observation window of 500 ps, a 2-to 3-fold decrease of the photoinduced response was observed in different experiments. The apparent time constant of the decay varied somewhat (≈70–200 ps), and actually the process may be nonexponential. We conclude that in at least half of the photolysed MV-CO complexes, subnanosecond geminate recombination of CO and heme *d* takes place.

Discussion

Contribution of Heme b_{595} to the Soret Band of the Reduced Cytochrome *bd*. Whereas the absorption characteristics of cytochrome *bd* in the α-, β-band region have been characterized earlier in detail,

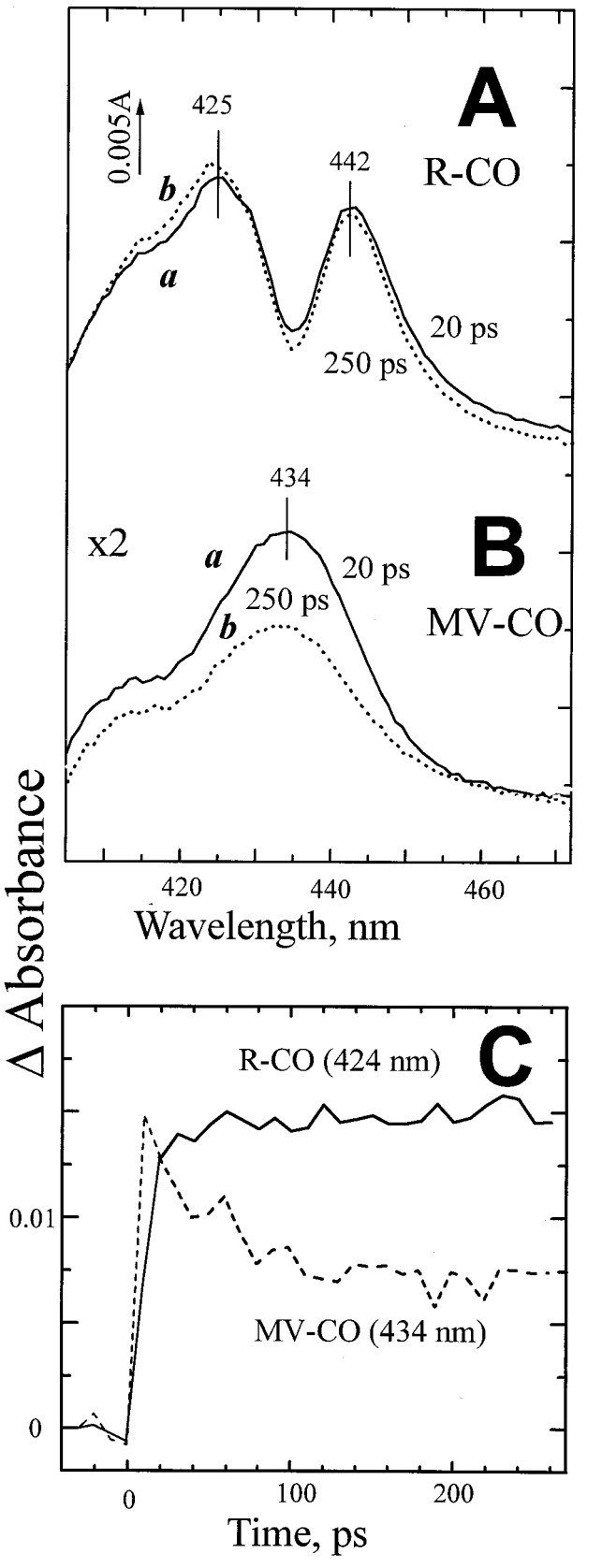

Fig. 2. Photodissociation of CO from the R (*A*) and MV states (*B*) of cytochrome *bd*. The absorption changes observed with the MV-CO complex have been expanded 2-fold. (*C*) Kinetics of the photoinduced changes in the two states. The responses have been normalized at $t = 20$ ps.

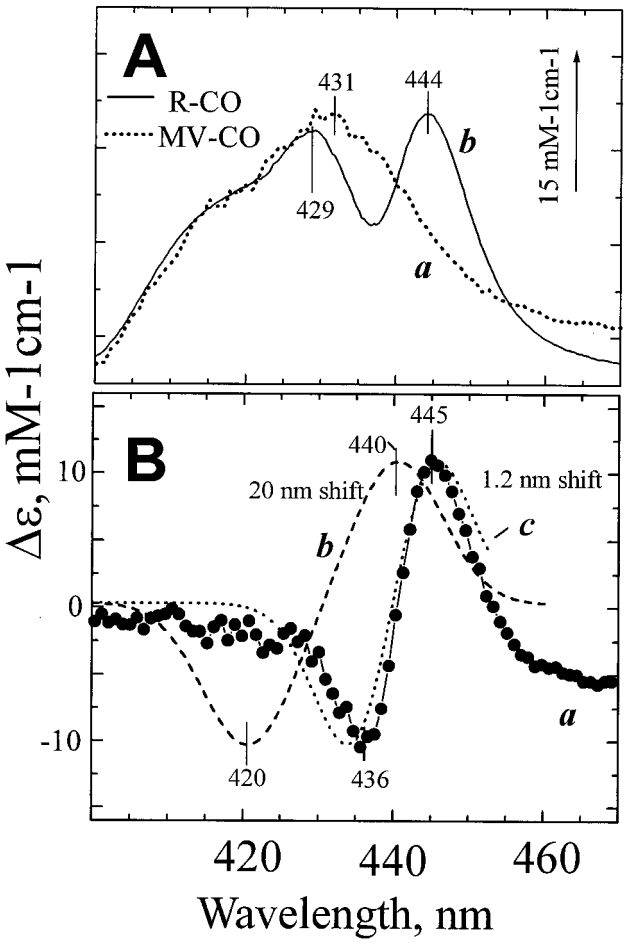

Fig. 3. A red shift of ferrous heme b_{595} absorption band induced by CO dissociation from heme *d*. (*A*) (*a*) Absorption changes induced by CO photodissociation from the MV and (*b*) static unliganded-CO − liganded spectrum of the R state (difference between curves *a* and *b* of Fig. 1*A*). The curves have been normalized by aligning their blue parts where they have similar line shapes. The scale bar refers to the R-CO state response. (*B*) Curve *a* gives the difference between spectra *b* and *a* in *A*. For comparison are shown simulated difference spectra for a 20-nm red shift corresponding to CO dissociation from heme b_{595} in ≈10% of cytochrome *bd* (*b*) and a 1.2-nm red shift of the entire population of b_{595} (*c*).

and the bands of hemes *d*, b_{595}, and b_{558} were identified (28, 31), the individual contributions of the three hemes to the Soret region have not been resolved (14). The absolute absorption spectrum of reduced cytochrome *bd* in the Soret region (Fig. 1*A*, curve *a*) is characterized by an asymmetric band with a maximum at ≈430 nm attributed provisionally to low-spin heme b_{558} (11, 14) and a shoulder around 440 nm, the origin of which is controversial. The absorption changes around 440 nm induced by binding of CO or NO to reduced cytochrome *bd* have been assigned earlier either to heme *d* (29, 30, 32) or heme b_{595} (11, 23). This work, exploiting the combination of selective heme excitation and ultrafast spectroscopy, provides direct evidence that the Soret shoulder at ≈440 nm corresponds to heme b_{595}. Identification of the heme b_{595} signature in the γ (Soret) region is essential for interpretation of the intricate spectral changes induced by binding of ligands, such as CO or NO, with the reduced enzyme.

Bandshift of Heme b_{595} Induced by CO Binding to Heme *d*. A major finding of this work is that the redox state of the *b*-type hemes strongly affects absorption changes induced by photodissociation of CO from heme *d*. As discussed below, this indicates proximity of hemes *d* and b_{595}.

The absorption changes induced by CO binding with fully reduced cytochrome *bd* are rather unusual. In the Q band region, CO brings about a red, rather than a conventional blue, shift of the well-resolved peak of ferrous heme *d* at about 628 nm, but does not affect significantly the band at 595 nm of heme b_{595}. In the Soret, a peculiar W-shaped trough with two well-resolved minima at ≈ 429 and 444 nm is observed (e.g., see Fig. 3*A*, curve *b*). This line shape has been amply discussed in the literature and sometimes is believed to report CO binding with both high-spin hemes *d* and b_{595} (refs. 14 and 23 and references therein).

Our data show that the W-shaped absorption changes in the Soret region are only induced by CO when the *b* hemes are reduced, but not in the MV state of the enzyme. Comparison of the difference spectra associated with CO binding to the R and MV states of cytochrome *bd* may allow resolving the specific spectral contribution from the reduced *b* hemes. As the immediate product of CO photodissociation from the fully reduced state shows additional contributions of unrelaxed states discussed below (Fig. 4), we first will compare the line shape of the MV-CO photodissociation spectrum with the conventional spectral changes induced by CO binding with fully reduced *bd* under static conditions.

Fig. 3*A* shows that in the R-CO difference spectrum, the spectral response of the MV-CO state, assigned provisionally to increased absorption of unliganded heme *d* at ≈431 nm, is superimposed by a narrow bandshift-type feature centered around 440–441 nm, as illustrated clearly by the difference between the normalized R-CO and MV-CO curves (Fig. 3*B*, curve *a*). It is this bandshift feature that confers the characteristic W-like shape to the CO- and NO-induced absorption changes in the reduced cytochrome *bd*. In principle, this contribution could reflect a perturbation of either low-spin heme b_{558} or high-spin heme b_{595}. Because the E_m values of the two *b* hemes are very

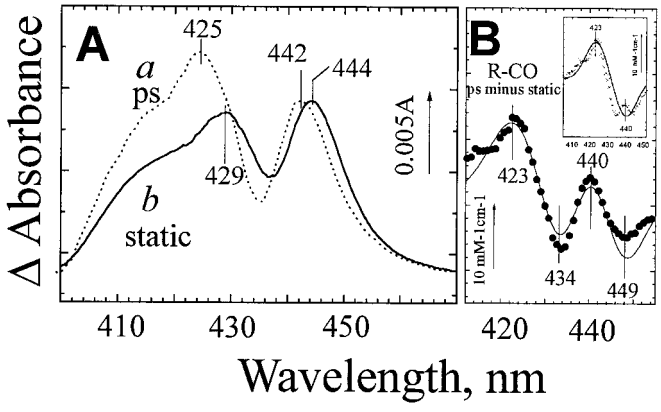

Fig. 4. Evidence for an unrelaxed intermediate state of ferrous heme b_{595} after CO photodissociation from heme *d*. (*A*) Absorption changes induced by CO dissociation from the R-CO state of cytochrome *bd* shortly after photolysis (*a*) and under static conditions (*b*). Curve *a* corresponds to the difference spectrum resolved by global analysis as a residual constant phase after relaxation of the excited states. Curve *b* is the difference spectrum (inverted) induced by addition of 20 μM CO to the fully reduced cytochrome *bd* (the same curve as in Fig. 3*A*). The spectra have been normalized by the height of the 442-to 444-nm peak. The ΔA scale bar refers to curve *a*. (*B*). The experimental difference between spectra *a* and *b* in *A* (●) has been simulated (the line) as narrowing of the b_{595} 440-nm band by 10% plus a 17-nm blue shift of this band in 10% of cytochrome *bd*. The Gaussian approximation of the band in Fig. 1*D* has been used for modeling. (*Inset*) After subtracting the contribution of b_{595} band narrowing, the difference between the picosecond and static CO photodissociation spectra (crosses) is dominated by the 17-nm blue shift of heme b_{595} (solid curve).

close (14) it is not possible to generate an equilibrium initial state of the enzyme with only one of the two hemes *b* reduced. However, the low-spin heme *b* is believed to have an absorption band at 429–430 nm (11, 14), whereas the band of heme b_{595} is located around 440 nm (this work). Accordingly, the position of the derivative-shaped feature centered at 440–441 nm strongly favors its interpretation as a red shift of ferrous heme b_{595}.

This small red shift may be explained either by CO-photodissociation from heme b_{595} in a small fraction of the enzyme, or by an indirect perturbation of the heme b_{595} Soret band induced by CO photodissociation from heme *d* (cf. ref. 23). The latter possibility is much more likely. First, we found the line shape of the Soret band changes associated with the ligand photodissociation in the R-CO state to be essentially the same for excitation at 653, 620, or 590 nm (data not shown). Were the response caused by CO photodissociation from heme b_{595}, a much lower relative contribution of this spectral perturbation would be expected for excitation at 653 or 620 nm as compared with 590 nm. Second, we have simulated spectrum *a* in Fig. 3*B* for different bandshifts, taking the line shape of the heme b_{595} absorption band from our photobleaching data. We assumed a provisional extinction coefficient of 150 $mM^{-1}{\cdot}cm^{-1}$ for the absorption maximum of ferrous b_{595}; this is a reasonable value for a high-spin heme γ-band (33) and it fits satisfactorily the absolute spectrum of the reduced cytochrome *bd*. CO binding to the heme iron is expected to shift the absorption band of a high-spin *b*-type heme to lower wavelengths by at least 10 nm (33, 34). A difference spectrum simulated for putative photodissociation of a b_{595}-CO complex assuming a 20-nm shift of heme b_{595} Soret band is shown in Fig. 3*B* (curve *b*). It is characterized by a maximum at ≈440 and a minimum at ≈420 nm, which agree reasonably well with the difference spectrum assigned to CO photodissociation from heme b_{595} at low temperatures (35, 36). Obviously, such a shift does not fit the line shape of the experimental spectrum (neither do smaller, 10- to 15-nm shifts, not shown). On the other hand, a good fit is obtained with respect to both size and line shape for a bandshift of the order of 1 nm (Fig. 3*B*, curve *c*).

Therefore we conclude that binding of CO to ferrous heme *d* in the fully reduced cytochrome *bd* perturbs the Soret absorption band of heme b_{595}. Such an effect points to an interaction between the two iron-porphyrin groups. A similar (although not identical, see below) shift is seen in the CO photodissociation difference spectrum of the fully reduced cytochrome *bd* a few ps after photodissociation (e.g., Figs. 2*A* and 4*A*). Therefore the heme-heme interactions are unlikely to be mediated by long-range slow conformational changes of the protein. Rather, the two hemes are in close proximity and communicate directly. Such communication could involve (*i*) excitonic interactions between the hemes and (*ii*) steric interactions. Concerning the first mechanism, it can be calculated by using the point dipole approximation for excitonic coupling (37) that for two hemes at a distance of 7 Å with heme planes at 55° (38); an 8% change in heme *d* oscillator strength would be sufficient to alter the interaction with heme b_{595} by ≈ 60 cm^{-1} (a shift of ≈1 nm at 440 nm). As to the second mechanism, bound CO could be sandwiched between the two hemes and thus sterically affect the heme b_{595} iron-macrocycle structure. For example, in the reduced bovine cytochrome *c* oxidase, the Fe_{a3}-Cu_B distance increases by ≈0.1 Å upon CO binding with heme a_3 (39).

Geminate Recombination of CO in the MV-CO Complex: Does Heme b_{595} Provide a Transient Binding Site for CO on its Way Out? The present work shows that at least half of the CO photodissociated from heme *d* in the MV-CO complex returns to heme *d* within a few hundred ps, presumably without leaving the heme pocket. In accordance with this finding, we have observed that the yield of CO photodissociation as measured on the millisecond time scale is significantly lower in the MV-CO complex than in the fully reduced CO complex (S. Siletsky, V.B.B., and A.A.K., unpublished work). We note that for no other heme protein, including cytochrome *c* oxidases aa_3 (40) and cbb_3 types (G. Lipowski, U.L., and M.H.V., unpublished work), significant geminate CO recombination on this time scale has been reported (in contrast to NO and O_2 that often show subnanosecond recombination; ref. 41).

Apparently, the redox state of hemes *b* (presumably b_{595}) controls the pathway by which CO escapes to the medium. A general possibility of such a control is that reduction of the *b* heme(s) results in a conformational change that opens an escape pathway or increases the probability/effective lifetime of opening of such a pathway driven by thermal fluctuations of the protein (e.g., see ref. 42). Specific channels conducting small substrates or product molecules like oxygen, hydrogen peroxide, and perhaps water to and from the heme active site have been discerned in many enzymes (ref. 43 and references therein), including cytochrome *c* oxidase aa_3 (39). More specifically, ferrous heme b_{595} may provide a transient binding site for the ligand on its way from heme *d* to the medium in analogy to Cu_B in the heme-copper oxidases (44). Because the ferric heme iron is not expected to be able to bind CO, the pathway will be blocked in the MV-CO state where heme b_{595} is oxidized.

Indications for transient binding of CO to b_{595} after ligand photodissociation from heme *d* in the fully reduced enzyme can be inferred from the spectral characteristics of the photodissociated state shortly after photolysis. Although the difference spectrum of CO photodissociation from reduced cytochrome *bd* observed on the picosecond time scale reproduces general features of the steady-state CO-dissociation spectrum, close comparison of these difference spectra shows that the line shapes are not identical (Fig. 4*A*). First, in the picosecond spectrum, the above-discussed b_{595} bandshift feature is displaced to the blue by ≈2 nm (maximum at 442 nm, minimum at 435 nm) relative to the static spectrum. Second, the picosecond curve reveals increased absorbance around 420 nm relative to the peak around 440 nm. Whereas the various reported static CO-induced difference spectra of cytochrome *bd* show some variation (23, 29, 45, 46), the long wavelength extreme at 443–445 nm is invariably more intense than the short wavelength one at 425–430 nm (Fig. 4, curve *a*). The same holds true for the difference spectrum of the rapid phase ($k \approx 10^8$ $M^{-1}{\cdot}s^{-1}$, $\tau_{obs} \approx 10^{-5}$ s) of bimolecular CO recombination with ferrous cytochrome *bd* at room temperature (ref. 30; S. Siletsky and V.B.B., unpublished work). Taken together, these results indicate the generation of a transient photodissociated state that is likely to relax within the 10^{-8}- to 10^{-5}-s time gap.

The difference between the picosecond and static difference spectra of CO dissociation from R-CO in Fig. 4*A* should reflect the difference between the spectra of the unliganded (R) states immediately after CO photodissociation and after relaxation. This difference (Fig. 4*B*, ●) reveals a rather complex pattern (the details of which depend somewhat on the normalization choice), that can be modeled qualitatively by two overlaying perturbations of heme b_{595}. Notably, the part of the difference spectrum in Fig. 4*B* above 430 nm with the peak at 440 nm and two minima on both sides of the peak can be modeled reasonably well with the second derivative of the b_{595} γ-absorption band at 440 nm, indicating that it reflects narrowing of the band. One interpretation of this narrowing is that a relatively well-defined conformation of the environment of heme b_{595} when CO is still in the heme pocket after photodissociation relaxes to a wider distribution of conformations upon escape of CO to the medium, and hence induces inhomogeneous broadening of its absorption band.

Subtraction of the second derivative-type contribution reveals a residual bandshift with a minimum at ≈440 nm and a maximum at ≈423 nm (Fig. 4*B Inset*) similar to that assigned

to CO binding with ferrous b_{595} (35, 36). Altogether, the basic features of the experimental absorption difference can be described by a contribution of (*i*) narrowing of the b_{595} band by ≈10% and (*ii*) a 17-nm blue shift in a small fraction (≈10%) of b_{595}. Thus the data are consistent with transient binding of photodissociated CO with heme b_{595} in a small fraction of the enzyme at room temperature. In combination with the effect of the redox state of heme b_{595} on rebinding of CO to heme *d,* an attractive hypothesis is that with reduced heme b_{595} a quasi-equilibrium between CO-liganded and unliganded heme b_{595} exists, which keeps CO near a potential escape pathway out of the protein.

CO binding to heme b_{595} upon photolysis of CO bound to heme *d* has been observed previously by Fourier transform IR spectroscopy at 20 K (19). At this temperature, CO binding to the heme is very slow (kiloseconds) (ref. 19 and cf. ref. 47). Our analysis indicates that the process also can take place at room temperature, speeding up to the picosecond range.

Concluding Remarks. We have exploited femtosecond optical spectroscopy to identify the spectral contribution of heme b_{595} in the Soret region and to study its role in ligand routing in cytochrome *bd*. The finding that heme b_{595} interacts with heme *d* on a picosecond time scale favors a di-heme oxygen reducing site in the *bd*-type oxidase; such an arrangement may facilitate trapping the oxygen and routing it toward the active site.

Note Added in Proof. The differences between the picosecond and static CO photodissociation spectra (Fig. 4) also could originate in the parallel polarization of the pump and probe pulses used in this work, as compared to unpolarized static absorption spectra. We recently performed polarized photoselection experiments, which indeed show that at least part of the spectral changes considered as evidence for transient CO binding with heme b_{595} can be accounted for by polarization effects. A preliminary analysis further strengthens the main assessment of the paper; i.e., a change in interaction between hemes *d* and b_{595} upon CO dissociation.

We are indebted to Dr. R. Gennis for the strain of *E. coli* GO 105/pTK1 and Dr. N. Yu. Safronova for growing the cells. The work was supported by an Action Spécifique avec les Pays d'Europe Centrale et Orientale grant from the Institut National de la Santé et de la Recherche Médicale, Grants 97–04-49765, 98–04-48847, and 99–04-48095 from the Russian Fund for Basic Research, and INTAS-Russian Fund for Basic Research Grant 95–1259. M.H.V. is supported by the Centre National de la Recherche Scientifique.

1. Ferguson-Miller, S. & Babcock, G. T. (1996) *Chem. Rev.* **96,** 2889–2908.
2. Mitchell, P. (1987) *FEBS Lett.* **222,** 235–245.
3. Mitchell, P. (1988) *Ann. N.Y. Acad. Sci.* **550,** 185–198.
4. Morgan, J. E., Verkhovsky, M. I. & Wikström, M. (1994) *J. Bioenerg. Biomembr.* **26,** 599–608.
5. Rich, P. R. (1991) *Biosci. Rep.* **11,** 539–571.
6. Wikström, M. (1998) *Biochim. Biophys. Acta* **1365,** 185–192.
7. Iwata, S., Ostermeier, C., Ludwig, B. & Michel, H. (1995) *Nature (London)* **376,** 660–669.
8. Michel, H. (1998) *Proc. Natl. Acad. Sci. USA* **95,** 12819–12824.
9. Osborne, J. P. & Gennis, R. B. (1999) *Biochim. Biophys. Acta* **1410,** 32–50.
10. Mogi, T., Tsubaki, M., Hori, H., Miyoshi, H., Nakamura, H. & Anraku, Y. (1998) *J. Biochem. Mol. Biol. Biophys.* **2,** 79–110.
11. Poole, R. K. (1988) in *Bacterial Energy Transduction*, ed. Anthony, C. (Academic, London), pp. 231–291.
12. Hill, B. C. (1993) *J. Bioenerg. Biomemb.* **25,** 115–120.
13. Puustinen, A., Finel, M., Haltia, T., Gennis, R. B. & Wikström, M. (1991) *Biochemistry* **30,** 3936–3942.
14. Junemann, S. (1997) *Biochim. Biophys. Acta* **1321,** 107–127.
15. Junemann, S., Wrigglesworth, J. M. & Rich, P. R. (1997) *Biochemistry* **36,** 9323–9331.
16. Poole, R. K. & Williams, H. D. (1987) *FEBS Lett.* **217,** 49–52.
17. Kobayashi, K., Tagawa, S. & Mogi, T. (1999) *Biochemistry* **38,** 5913–5917.
18. Krasnoselskaya, I., Arutjunjan, A. M., Smirnova, I., Gennis, R. & Konstantinov, A. A. (1993) *FEBS Lett.* **327,** 279–283.
19. Hill, J. J., Alben, J. O. & Gennis, R. B. (1993) *Proc. Natl. Acad. Sci. USA* **90,** 5863–5867.
20. Vos, M. H. & Martin, J.-L. (1999) *Biochim. Biophys. Acta* **1411,** 1–20.
21. Kaysser, T. M., Ghaim, J. B., Georgiou, C. & Gennis, R. B. (1995) *Biochemistry* **34,** 13491–13501.
22. Miller, M. J. & Gennis, R. B. (1986) *Methods Enzymol.* **126,** 87–94.
23. Borisov, V., Arutyunyan, A. M., Osborne, J. P., Gennis, R. B. & Konstantinov, A. A. (1999) *Biochemistry* **38,** 740–750.
24. Martin, J.-L. & Vos, M. H. (1994) *Methods Enzymol.* **232,** 416–430.
25. Liebl, U., Lambry, J.-C., Leibl, W., Breton, J., Martin, J.-L. & Vos, M. H. (1996) *Biochemistry* **35,** 9925–9934.
26. Petrich, J. W., Poyart, C. & Martin, J.-L. (1988) *Biochemistry* **27,** 4049–4060.
27. Yonetani, T. & Ray, G. S. (1965) *J. Biol. Chem.* **240,** 4503–4508.
28. Lorence, R. M., Koland, J. G. & Gennis, R. B. (1986) *Biochemistry* **25,** 2314–2321.
29. Junemann, S. & Wrigglesworth, J. M. (1995) *J. Biol. Chem.* **270,** 16213–16220.
30. Junemann, S., Rich, P. R. & Wrigglesworth, J. M. (1995) *Biochem. Soc. Trans.* **23,** 157S.
31. Koland, J. G., Miller, M. J. & Gennis, R. B. (1984) *Biochemistry* **23,** 1051–1056.
32. Kauffman, H. F., van Gelder, B. F. & DerVartanian, D. V. (1980) *J. Bioenerg. Biomembr.* **12,** 265–276.
33. Wood, P. M. (1984) *Biochim. Biophys. Acta* **768,** 293–317.
34. Poole, R. K. (1994) in *Chemical Methods in Prokaryotic Systematics*, eds. Goodfellow, M. & O'Donnell, A. G. (Wiley, New York), pp. 311–344.
35. D'mello, R., Palmer, S., Hill, S. & Poole, R. K. (1994) *FEMS Microbiol. Lett.* **121,** 115–120.
36. D'mello, R., Hill, S. & Poole, R. K. (1996) *Microbiology* **142,** 755–763.
37. Pearlstein, R. M. (1987) in *Photosynthesis*, ed. Amesz, J. (Elsevier, Amsterdam), pp. 299–317.
38. Ingledew, W. J., Rothery, R. A., Gennis, R. B. & Salerno, J. C. (1992) *Biochem. J.* **282,** 255–259.
39. Yoshikawa, S., Shinzawa-Itoh, K., Nakashima, R., Yaono, R., Yamashita, E., Inoue, N., Yao, M., Fei, M. J., Libeu, C. P., Mizushima, T., *et al*. (1998) *Science* **280,** 1723–1729.
40. Stoutland, P. O., Lambry, J.-C., Martin, J.-L. & Woodruff, W. H. (1991) *J. Phys. Chem.* **95,** 6406–6408.
41. Martin, J.-L. & Vos, M. H. (1992) *Annu. Rev. Biophys. Biomol. Struct.* **21,** 199–222.
42. Perutz, M. F. & Mathews, F. S. (1966) *J. Mol. Biol.* **21,** 199–202.
43. Bravo, J., Mate, M. J., Schneider, T., Switala, J., Wilson, K., Loewen, P. C. & Fita, I. (1999) *Proteins* **34,** 155–166.
44. Einarsdóttir, O. (1995) *Biochim. Biophys. Acta* **1229,** 129–147.
45. Miller, M. J. & Gennis, R. B. (1983) *J. Biol. Chem.* **258,** 9159–9165.
46. Kita, K., Konishi, K. & Anraku, Y. (1984) *J. Biol. Chem.* **259,** 3375–3381.
47. Frauenfelder, H., Sligar, S. G. & Wolynes, P. G. (1991) *Science* **254,** 1598–1603.